

Determining spectral response of the National Ignition Facility particle time of flight diagnostic to x rays

Cite as: Rev. Sci. Instrum. **94**, 033510 (2023); <https://doi.org/10.1063/5.0101725>

Submitted: 03 June 2022 • Accepted: 28 February 2023 • Published Online: 22 March 2023

 B. Reichelt,  N. Kabadi,  J. Percy, et al.

COLLECTIONS

Paper published as part of the special topic on [Proceedings of the 24th Topical Conference on High-Temperature Plasma Diagnostics](#)



View Online



Export Citation



CrossMark

ARTICLES YOU MAY BE INTERESTED IN

[Neutron imaging of inertial confinement fusion implosions](#)



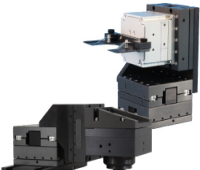
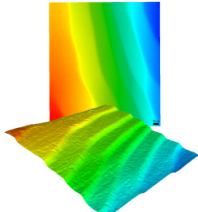
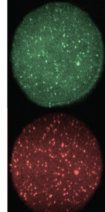
Review of Scientific Instruments **94**, 021101 (2023); <https://doi.org/10.1063/5.0124074>

[Charged particle diagnostics for inertial confinement fusion and high-energy-density physics experiments](#)

Review of Scientific Instruments **94**, 021104 (2023); <https://doi.org/10.1063/5.0127438>

[Soft x-ray power diagnostics for fusion experiments at NIF, Omega, and Z facilities](#)

Review of Scientific Instruments **94**, 031101 (2023); <https://doi.org/10.1063/5.0131949>

 MCL MAD CITY LABS INC. www.madcitylabs.com	<p>Nanopositioning Systems</p> 	<p>Modular Motion Control</p> 	<p>AFM and NSOM Instruments</p> 	<p>Single Molecule Microscopes</p> 
---	--	--	---	--

Determining spectral response of the National Ignition Facility particle time of flight diagnostic to x rays

Cite as: Rev. Sci. Instrum. 94, 033510 (2023); doi: 10.1063/5.0101725

Submitted: 3 June 2022 • Accepted: 28 February 2023 •

Published Online: 22 March 2023



View Online



Export Citation



CrossMark

B. Reichelt,^{1,a)} N. Kabadi,¹ J. Pearcy,¹ M. Gatu Johnson,¹ S. Dannhoff,¹ B. Lahmann,¹ J. Frenje,¹ C. K. Li,¹ G. Sutcliffe,¹ J. Kunimune,¹ R. Petraso,¹ H. Sio,² A. Moore,² E. Mariscal,² and E. Hartouni²

AFFILIATIONS

¹Massachusetts Institute of Technology, Cambridge, Massachusetts 02139, USA

²Lawrence Livermore National Laboratory, Livermore, California 94550, USA

Note: This paper is part of the Special Topic on Proceedings of the 24th Topical Conference on High-Temperature Plasma Diagnostics.

^{a)}Author to whom correspondence should be addressed: blr@mit.edu

ABSTRACT

The Particle Time of Flight (PTOF) diagnostic is a chemical vapor deposition diamond detector used for measuring multiple nuclear bang times at the National Ignition Facility. Due to the non-trivial, polycrystalline structure of these detectors, individual characterization and measurement are required to interrogate the sensitivity and behavior of charge carriers. In this paper, a process is developed for determining the x-ray sensitivity of PTOF detectors and relating it to the intrinsic properties of the detector. We demonstrate that the diamond sample measured has a significant non-homogeneity in its properties, with the charge collection well described by a linear model $ax + b$, where $a = 0.63 \pm 0.16 \text{ V}^{-1} \text{ mm}^{-1}$ and $b = 0.00 \pm 0.04 \text{ V}^{-1}$. We also use this method to confirm an electron to hole mobility ratio of 1.5 ± 1.0 and an effective bandgap of 1.8 eV rather than the theoretical 5.5 eV, leading to a large sensitivity increase.

Published under an exclusive license by AIP Publishing. <https://doi.org/10.1063/5.0101725>

I. INTRODUCTION

The Particle Time of Flight (PTOF) diagnostic is a diagnostic routinely utilized for measuring the time of peak nuclear emission for low yield implosions at the National Ignition Facility (NIF).¹ PTOF relies upon a gold-coated chemical vapor deposition (CVD) grown diamond that has a bias held across it. Diamond is a good choice of detector in high energy density physics as its high bandgap of 5.5 eV and strong interatomic bonds lead to impressive radiation hardness and low leakage currents.^{2,3} When ionizing radiation interacts with the biased diamond, an electron-hole pair is freed into the conduction/valence band, respectively. These freed charges are now mobile and are swept in opposite directions by the bias, where they will induce a surface charge on the gold electrode and will either eventually recombine or get absorbed into the electrode. In either case, the resulting charges on the electrode will induce a change in voltage that can be read via an oscilloscope.

Despite being used for proton and neutron signals, PTOF is also sensitive to x rays. This fact is important when choosing the filtering since an x-ray signal that is too large can lead to saturation and the loss of the nuclear signal. Having an absolute calibration of the sensitivity to x rays will aid with filter selection and ensure data remains analyzable. Additionally, a better understanding of how PTOF reacts to x rays enhances the possibility of using PTOF for x-ray bang time information.

The x-ray response of PTOF also provides information about the behavior of charge carriers in CVD diamonds, which is important for gaining a more accurate understanding of how the response of PTOF varies for different ionizing radiation. Most pertinently, neutrons deposit their energy volumetrically throughout the detector, whereas charged particles and x rays deposit more energy at the front of the detector since they are significantly attenuated by the diamond. The standard PTOF detector is biased at $0.5 \text{ V}/\mu\text{m}$ with a $1000 \mu\text{m}$ thickness, which is significantly more than the charge

collection distance,³ meaning that the region in which energy is deposited can significantly alter the sensitivity and falling edge of the impulse response.

II. SOURCE CHARACTERIZATION

To test x-ray sensitivity, a Proto x-ray cabinet (<https://www.protoxrd.com>) was used along with custom-machined hardware to mount the PTOF detector and an x-ray spectrometer. The x rays are generated by thick target bremsstrahlung of an electron beam with known energy and current. As the x rays exit the source window, they pass through a hole in a shielding plate 16 cm below the source, where they are filtered and collimated to obtain an appropriate photon flux for measurement (see Fig. 1). The collimators used are made of the tungsten based alloy HD17 and range in thickness from 1 to 2 mm, and filtering was provided by well characterized aluminum disks of various thicknesses. Previous work using image plates has shown the source to be uniform within the collimated area. After passing through the filtering and collimation, the x rays deposit their energy in either a PTOF detector or a calibrated spectrometer, which can easily be swapped out for each other. The collimation is chosen to ensure that the imaged source size on both devices is smaller than the active area of each device, ensuring accurate conversion between spectra measured by the spectrometer and those absorbed by the PTOF detector.

The PTOF detector tested utilizes a 10 mm diameter, 1 mm thick microwave plasma grown CVD diamond biased at 500 V. The “normal” bias direction is taken to be such that the front of the diamond facing the x-ray source has a higher potential than the rear face. The diamond comes with a 9 mm diameter metallization for biasing purposes on both sides, consisting of 100 nm Ti for diamond adhesion, 200 nm Pt to inhibit diffusion from Ti into Au, and 1000 nm of Au to act as an electrode. Current through the PTOF detector at a given bias and x-ray spectrum was measured with a Keithley multi-meter. To probe response at different x-ray energies, a variety of sources, filtering, and electron beam voltages were utilized.

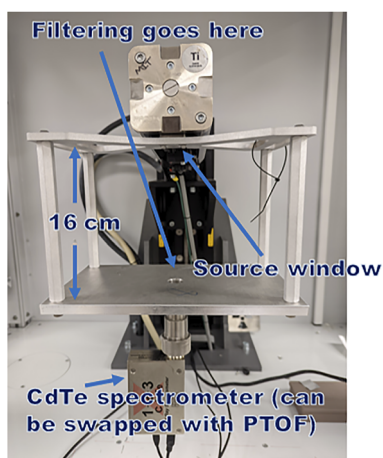


FIG. 1. Picture of the experimental setup, showing the x-ray source and hardware used to mount the spectrometer and PTOF detector in the same location.

The spectra utilized in the analysis were measured with an Amptek X-123 CdTe spectrometer (<https://www.amptek.com>) mounted in nearly the same location as the PTOF detector. Energy axis calibration was achieved with a ²⁴¹Am source. Ideally, the spectrometer would be run with the exact same collimation and x-ray source current as the PTOF detector. Unfortunately, the precision of our electrometer was too low for this to be practical since currents that were large enough to measure on the PTOF detector with the multimeter led to extreme pile-up on the spectrometer. Thus, the initial step in the analysis was to relate the magnitude of the spectrum to the collimation and x-ray source current used and to ensure that spectral shape was not significantly altered by changing these parameters.

Finding the scaling of the spectral magnitude with collimator size and x-ray source current involves a maximum likelihood fit between two spectra—the unscaled “reference spectrum” and the “scaled spectrum.” Specifically, we take the high statistic reference spectrum and smooth it slightly with a Gaussian filter before dividing it by the live time in order to get a reference count rate for each bin. The desired scaling is applied by multiplying this reference rate by the scale factor *A* and fitting it to the scaled spectrum until Poisson distributed log-likelihood is maximized. An example of scaled spectra is given in Fig. 2, where spectra taken with varying collimation and x-ray source current have been scaled to match a reference spectrum using the above process. Figure 2 demonstrates that aside from the 25 μm collimation, the spectral shape is conserved with different collimators.

The results from scaling the source current and collimator diameter are shown in Fig. 3. It can be seen that the count rate for the Cu tube scales very linearly with the x-ray source current, with a Pearson correlation coefficient of 0.999 989 (the Ti tube has a similar result). This simplifies conversion between spectrometer spectra and those incident upon the CVD diamond when they are taken at different source currents.

Meanwhile, the scaling for collimator size deviates much more noticeably from the quadratic scaling that would be expected from a point source. However, aside from the 25 μm collimator on the Cu tube, the shapes of all spectra match very well, and the deviations from quadratic scaling are well reproduced when changing

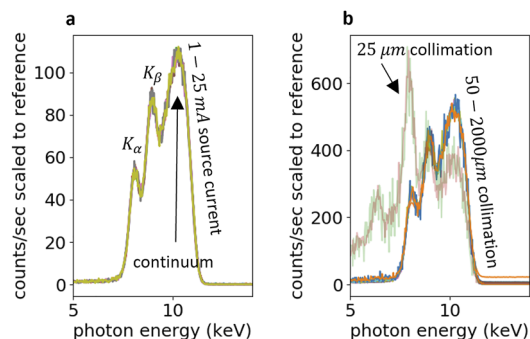


FIG. 2. Spectra scaled to match reference spectrum for Cu source with 140.1 mg/cm² Al filtering, varying (a) source current from 1 to 25 mA and (b) collimation diameter from 25 to 2000 μm . Spectral shape is evidently independent of these parameters outside of 25 μm collimation.

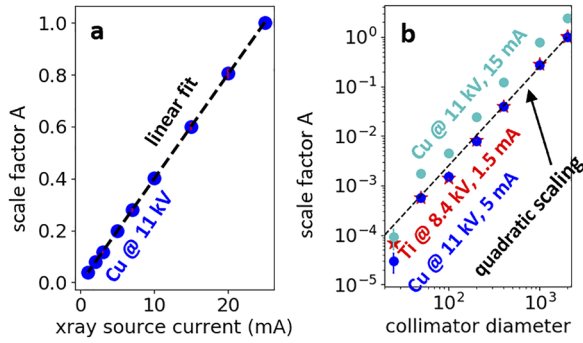


FIG. 3. Measured scalings of x-ray spectra vs (a) x-ray source current, and (b) collimator diameter. Note that the Cu points use Cu @ 11 kV, 5 mA with 2000 μm collimation as the reference, while the Ti points use Ti @ 8.4 kV, 1.5 mA with 2000 μm collimation as a reference.

source type, current, and voltage. The consistent nature of the shifts suggests some combination of finite source size effects that are consistent between tubes and deviations in the collimator diameter from the nominal values.

The outliers are the 25 μm collimators on the Cu tube, which had much lower count rates than expected and significantly distorted spectra. The most likely reason for this is that with an aspect ratio of 0.023, the smallest collimators were imaging an area with a radius of ~ 3 mm—a size slightly smaller than the x-ray window size and less than half the radius imaged by all the other collimators. This made it extremely susceptible to misalignment, as only a 1° change could result in entirely missing the window. To aid with this, a smaller separation between the source and collimator stage will be used in future tests. To avoid this issue, on the current dataset, only spectra taken with ≥ 50 μm collimation are used.

III. METHODOLOGY

The goal of these measurements is to determine the sensitivity of the PTOF detector, given some x-ray flux. To do this, we measure the current flowing through the detector over a series of steps in the x-ray source current, giving the detector ~ 50 s to equilibrate at each step. An example output trace is shown in Fig. 4. Ultimately, the current going through the detector, I_{PTOF} , is a function of the free carriers in the diamond,

$$I_{PTOF} = qA[v_e(n_e^{v,y} + n_e^{t,y} + n_e^{f,0}) + v_h(n_h^{c,y} + n_h^{t,y} + n_h^{f,0})], \quad (1)$$

with q being the electron charge, A being the cross-sectional area where carriers are present, and $v_{e(h)}$ being the electron (hole) velocity, which is a function of the electric field. The total free electron (hole) densities n_e and n_h are split into three components each: $n_{e(h)}^{v(c),y}$ denotes the density of electrons (holes) excited by x rays from the valence (conduction) band to become free charge carriers, $n_{e(h)}^{t,y}$ denotes the density of electrons (holes) excited by x rays from deeply trapped states to become free charge carriers, and $n_{e(h)}^{f,0}$ denotes the free carriers that are present when no x rays illuminate the diamond through thermal effects and shallow traps. All of the carrier parameters can be functions of location within the detector since

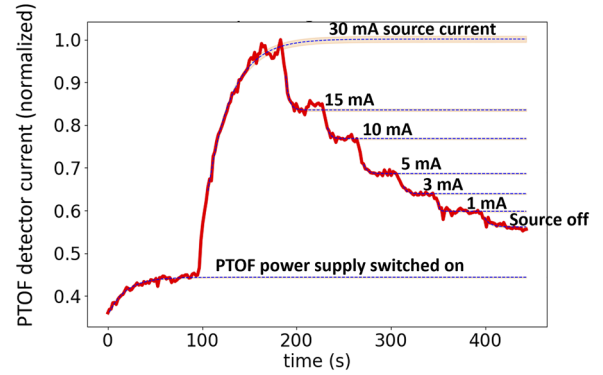


FIG. 4. Example trace of current through PTOF diamond. The x-ray source current is varied in steps, and the PTOF current is given time to equilibrate at each step before being measured.

they depend upon the local mobility and recombination rate of the diamond.

The $n_{e(h)}^{f,0}$ terms provide a continuous dark current so they are not of primary interest for determining detector sensitivity to photons. Figure 4 displays an Example PTOF current trace used for the analysis—the initial curve when the PTOF bias is applied demonstrates this dark current.

The $n_{e(h)}^{v(c),y}$ terms are the ones we are most interested in since they provide the bulk of the charge carriers for high amplitude signals and scale linearly with x-ray flux,⁴

$$n_{e(h)}^{v(c),y} = \frac{\tau_{e(h)} dP/dx}{A\epsilon}, \quad (2)$$

where x is the distance from the front of the diamond, $\tau_{e(h)}$ is carrier lifetime, A is detector area, and $dP/dx = \int_0^\infty P_0(E) e^{-\mu_C(E)x} \mu_C(E) dE$ is x-ray power absorbed per dx at position x , given an initial spectrum P_0 at the front of the diamond and an x-ray attenuation factor⁵ μ_C . Finally, ϵ is the number of eV required to free an electron-hole pair (previous analyses suggest 13 eV for diamond⁶).

The $n_{e(h)}^{t,y}$ terms pose some difficulty since they obey a nonlinear rate equation,³

$$\frac{dn_{e(h)}^{t,y}}{dt} = -\left(n_{e(h)}^{t,y} + n_{e(h)}^{v(c),y}\right) n_{e(h)}^{t,y} \alpha^{RT} + \left(T - n_{e(h)}^{t,y}\right) \frac{dP}{dx} \alpha^{DT}, \quad (3)$$

where α^{RT} and α^{DT} are the factors of the re-trapping and de-trapping frequencies that are not dependent on any carrier densities or x-ray flux, respectively, and T is the total density of trapped states. Guidance for analyzing this component can be found by considering the equilibrium solution,

$$n_{e(h)}^{t,y} = \frac{1}{2} \sqrt{\left[\frac{dP}{dx} \left(\frac{\alpha^{DT}}{\alpha^{RT}} + \frac{\tau_{e(h)}}{A\epsilon} \right) \right]^2 + 4T \frac{dP}{dx} \alpha^{DT}} - \frac{1}{2} \frac{dP}{dx} \left(\frac{\alpha^{DT}}{\alpha^{RT}} + \frac{\tau_{e(h)}}{A\epsilon} \right). \quad (4)$$

We can see that for larger x-ray fluxes, this asymptotes to a value independent of x-ray flux, but at lower x-ray flux, it quickly

approaches zero. This is exactly the behavior seen in Fig. 4: when the source is turned off, the current decays all the way down to the asymptotic dark current reached when turning on the power supply, albeit very slowly. Separate tests running for long periods of time have confirmed this experimentally. The slow decay at the end agrees with Eq. (3), which predicts a $1/t$ decay rather than an exponential once $dP/dx = 0$. Fully decoupling this term from the $n_{e(h)}^{v(c),\gamma}$ terms is difficult, but provided there is a large enough x-ray flux to saturate the trapped state component, it can essentially be absorbed into the intrinsic carrier population $n_{e(h)}^{f,0}$. Thus, we can write a linear relationship between current and power,

$$I_{PTOF} = \frac{q}{D} \int_0^D \frac{d(x)}{\epsilon(x)} \frac{dP}{dx} dx + I_{dark} \left(\int_0^t P(t') dt' \right), \quad (5)$$

where the first term comes from spatially averaging Eq. (1) over the diamond to get a spatially averaged charge collection $(qd/\epsilon D)_x$, and the dark current is now a complex function of the total irradiation but remains nearly constant over each current trace when the source is on. D is the detector thickness, and d is the charge collection distance, which is nominally equal to $n_e^{v,\gamma} v_e + n_h^{c,\gamma} v_h$ but can deviate from this value near the contacts or in regions of strongly varying $v_{e(h)}$ or $n_{e(h)}^{v(c),\gamma}$.

In order to probe the detector response thoroughly, experimentation was done to find a combination of filterings and sources to create spectra with a variety of peaks. Smaller peaks are desirable to reduce analysis degeneracy but limitations on x-ray sources available to us necessitated filtering the continuum emission to get higher energy peaks. Figure 5 demonstrates the shape of the spectra used to determine sensitivity, as well as linear fits⁷ relating source current to $I_{PTOF} - I_{dark}$ in the vein of Eq. (5). Given the discussion of Eq. (4), linear fits are taken only with the higher flux data points where possible to ensure saturation of trapped carriers. The discussion of trapped carriers is likely responsible for the notable difference in dark current between the Cu source and Ti sources since that run was the first on the next day, after a large number of freed traps from

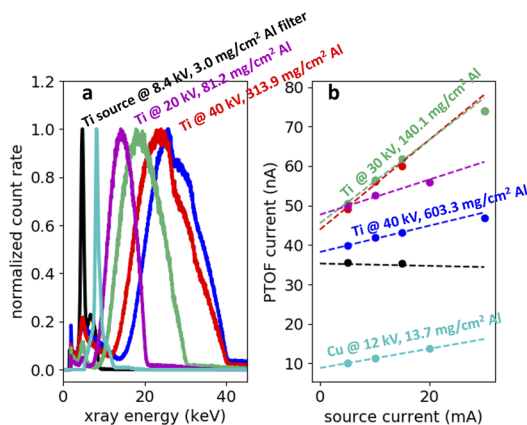


FIG. 5. Example illustrating (a) normalized x-ray spectra and (b) the corresponding PTOF currents. PTOF currents are plotted against a linear fit to the higher flux data points, following the discussion of Eq. (4). This fit is used to determine spectrally averaged sensitivity.

heavy irradiation the day prior had time to recombine. Evidently, the x-ray flux for this shot alone was not high enough to re-saturate the freed traps over the course of the run.

IV. RESULTS

Using Eq. (5), it is straightforward to postulate a linear charge collection model: $qd/\epsilon D = ax + b$. Combining with the formula for dP/dx , the spatially averaged charge collection becomes equivalent to a spectral average of the model sensitivity $S(E)$,

$$\left\langle \frac{qd}{\epsilon D} \right\rangle_x = \langle S \rangle_E = \int_0^\infty P_0 S(E) dE / \int_0^\infty P_0 dE \quad (6)$$

with $S(E) = (1 - e^{-\mu_c D}) [a\mu_c^{-1} + b] - aDe^{-\mu_c D}$. However, we also know that the experimental sensitivity $(I_{PTOF} - I_{dark}) / \int_0^\infty P_0 dE$ is a constant given by the lines fit in Fig. 5(b) after some conversion to get from spectrometer measured spectra to those incidents on PTOF using methods from Sec. II. The end result is that given a choice of a and b , we can see how well the averaged model sensitivities match the experimental values and then perform a χ^2 minimization routine to select the optimal parameters.

The reasoning behind this linear charge collection model is that the diamond is not a perfect crystal—there are defects, impurities, and grain boundaries that alter the effective bandgap and inhibit carrier movement.³ The growth process for diamonds specifically results in an inhomogeneous structure as grain size grows from the nucleation side out. The best fit to a linear charge collection model leads to the blue model sensitivity curve and green averaged model sensitivities in Fig. 6. It can be seen that this does a good job of matching the experimental sensitivities, which are plotted against the averaged absorbed photon energy for the spectrum. Error bars from the experimental sensitivities come from the errors in the linear fits of source current vs detector sensitivity. This is added in quadrature with a 50% error attributed to the subtleties of Eq. (4) that were sidestepped to get a linear fit—experimentation with fits to this equation assuming a simpler homogeneous model revealed departures less than or similar to this from the linear fit. The exception is the Ti source @ 8.4 kV with 3.0 mg/cm² Al filtering, whose error bar was chosen to match the signal level of the next smallest signal since it was at the noise floor, and no discernible signal was present when the source was on.

The linear charge collection model $(q/D)(d/\epsilon) = ax + b$ has a best fit value of $a = 0.63 \pm 0.16 \text{ V}^{-1} \text{ mm}^{-1}$ and $b = 0.00 \pm 0.04 \text{ V}^{-1}$, indicating that spatial inhomogeneities are significant within this sample and suggesting that the nucleation side of the diamond was the side facing the x-ray source. It is also clear that there are significant impurities and grain boundaries causing an effective modification of the bandgap^{8,9}—the standard value of q/ϵ in diamond is 0.077 V^{-1} , but this is exceeded by the end of the diamond where $(q/D)(d/\epsilon) \approx 0.6 \text{ V}^{-1}$. d/D must be less than unity, so the only way this can occur is if ϵ is smaller than usual owing to impurities. In fact, the difference is likely even more dramatic, as the usual values for carrier mobility and lifetimes in diamond^{4,6} lead to $d/D \approx 0.1$. This is supported by the values of dark current observed: $I_{dark} \approx 10 \text{ nA} \approx 2qAv_e (m_e k_B T / 2\pi\hbar^2)^{3/2} \exp(-E_g/2k_B T)$ leads to a value of $E_g \approx 1.8 \text{ eV}$ rather than 5.5 eV.

Finally, one last notable feature of the data shown in Fig. 6 is the discrepancy between the forward and reverse bias configurations.

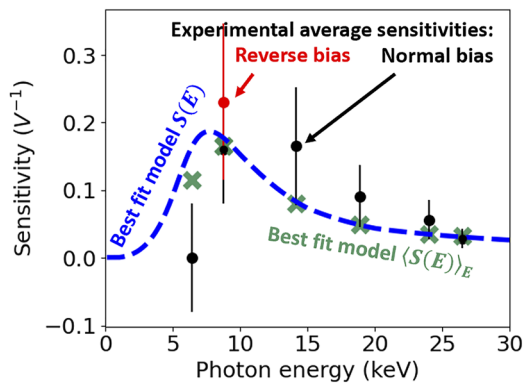


FIG. 6. Experimental sensitivities plotted vs mean absorbed photon energy for different spectra are plotted as circular points. Shown in blue is the best fit model sensitivity curve $S(E)$, with the green x's being the spectrally averaged values. All measured spectra are corrected for attenuation through the contacts before being analyzed for sensitivity.

In the forward bias configuration, the side nearest the source is biased higher than the rear side of the diamond. As just shown, there is greater carrier mobility at the rear side of the diamond, so in the normal bias configuration, the holes are moving in the direction of increasing mobility and lifetime, whereas the electrons are doing the opposite and so will recombine more quickly. The opposite is, of course, true for the reverse bias situation, and so the increased sensitivity is likely a result of greater electron mobility and lifetime. Taking an extreme model where $v_{e(h)}\tau_{e(h)} = 0$ in the forward (reverse) bias case so that $d \approx v_{h(e)}\tau_{h(e)}$, we obtain the charge collection ratio $v_e\tau_e/v_h\tau_h \approx 1.5 \pm 1.0$ —in alignment with the ratio of electron to hole mobility discussed in the literature.^{4,6}

V. CONCLUSION AND PATH FORWARD

In conclusion, we have developed an in-house method for probing the behavior of PTOF detectors with x rays. Results with the currently available detector show much higher sensitivity than expected, which is consistent with impurities introducing additional states for charge carriers within the bandgap of the diamond. We also demonstrate the efficacy of a linear model in describing the charge collection of the diamond and provide a framework to disentangle the contributions of several different carrier species that contribute to x-ray response.

In the future, this process will be used to characterize both new and used PTOF detectors and perform quality assurance. Additionally, experiments are currently under way to probe the impulse response of these detectors using ultra short electron bunches at the LLNL xband facility. These tests will allow for the characterization of carrier lifetimes, providing further insight into the mechanisms that alter sensitivity to low energy x rays. Future efforts will also be directed toward the intricacies of Eq. (3) and lowering the error of this analysis through a combination of analytical models and improved equipment.

ACKNOWLEDGMENTS

This work was supported by the DOE/NNSA CoE under Contract No. DE-NA0003868 and the LLNL under Contract No.

B640112. B. Reichelt is supported by the NNSA SSGF under Grant No. DE-NA0003960. Approved for unlimited release with Release No. LLNL-JRNL-835720.

AUTHOR DECLARATIONS

Conflict of Interest

The authors have no conflicts to disclose.

Author Contributions

B. Reichelt: Conceptualization (equal); Data curation (lead); Formal analysis (lead); Investigation (lead); Methodology (lead); Validation (lead); Visualization (lead); Writing – original draft (lead); Writing – review & editing (lead). **N. Kabadi:** Conceptualization (equal); Methodology (supporting). **J. Pearcy:** Data curation (supporting). **M. Gatu Johnson:** Conceptualization (supporting); Funding acquisition (equal); Writing – review & editing (supporting). **S. Dannhoff:** Data curation (supporting); Validation (supporting). **B. Lahmann:** Validation (supporting). **J. Frenje:** Funding acquisition (equal); Validation (supporting); Writing – review & editing (supporting). **C. K. Li:** Funding acquisition (equal); Supervision (supporting). **G. Sutcliffe:** Validation (supporting); Writing – review & editing (supporting). **J. Kunimune:** Data curation (supporting); Validation (supporting). **R. Petrasso:** Funding acquisition (equal); Resources (equal). **H. Sio:** Validation (supporting); Writing – review & editing (supporting). **A. Moore:** Resources (supporting); Validation (supporting); Writing – review & editing (supporting). **E. Mariscal:** Resources (supporting); Validation (supporting). **E. Hartouni:** Validation (supporting).

DATA AVAILABILITY

The data that support the findings of this study are available from the corresponding author upon reasonable request.

REFERENCES

- H. G. Rinderknecht *et al.*, “A novel particle time of flight diagnostic for measurements of shock- and compression-bang times in D^3He and DT implosions at the NIF,” *Rev. Sci. Instrum.* **83**, 10D902 (2012).
- C. J. H. Wort and R. S. Balmer, “Diamond as an electronic material,” *Mater. Today* **11**, 22–28 (2008).
- D. Meier, “CVD diamond sensors for particle detection and tracking,” Ph.D. thesis, Heidelberg University, 1999.
- D. R. Kania *et al.*, “Absolute x-ray power measurements with subnanosecond time resolution using type IIa diamond photoconductors,” *J. Appl. Phys.* **68**, 124–130 (1990).
- R. T. Berger, “The X- or gamma-ray energy absorption or transfer coefficient: Tabulations and discussion,” *Radiat. Res.* **15**, 1–29 (1961).
- C. Canali *et al.*, “Electrical properties and performances of natural diamond nuclear radiation detectors,” *Nucl. Instrum. Methods* **160**, 73–77 (1979).
- P. Virtanen *et al.*, “SciPy 1.0: Fundamental algorithms for scientific computing in Python,” *Nat. Methods* **17**, 261–272 (2020).
- A. S. Moore *et al.*, “Soft x-ray measurements using photoconductive type-IIa and single-crystal chemical vapor deposited diamond detectors,” *Rev. Sci. Instrum.* **79**, 10E923 (2008).
- H. F. Haneeff, A. M. Zeidell, and O. D. Jurchescu, “Charge carrier traps in organic semiconductors: A review on the underlying physics and impact on electronic devices,” *J. Mater. Chem. C* **8**, 759–787 (2020).